Journal of Magnetic Resonance 307 (2019) 106579

Contents lists available at ScienceDirect

Journal of Magnetic Resonance

journal homepage: www.elsevier.com/locate/jmr

MRI and localised NMR spectroscopy of sessile droplets on hydrophilic, hydrophobic and superhydrophobic surfaces – Examination of the chemical composition during evaporation

J. Kind *, C.M. Thiele

Clemens-Schöpf-Institut für Organische Chemie und Biochemie, Technische Universität Darmstadt, Alarich-Weiss-Str. 16, D-64287 Darmstadt, Germany

A R T I C L E I N F O

Article history:
Received 3 July 2019
Revised 15 August 2019
Accepted 16 August 2019
Available online 17 August 2019

Keywords:
Magnetic resonance imaging
Droplet evaporation
Chemical composition
Localised spectroscopy
Surface

A B S T R A C T

Evaporation of droplets is a process important in many different areas of science, technology and also everyday life. The understanding of droplet evaporation of homogeneous and heterogeneous substance mixtures is important, for example, to explain the formation of coffee stains or to optimize the results in offset printing. For a detailed understanding of the evaporation of complex mixtures from structured surfaces, such as inks used in offset printing, a time-resolved analysis of the droplet composition is essential. Measurement of (local) concentrations may deepen the understanding of wetting phenomena and their connection with transport phenomena.

Therefore, we demonstrate in this paper that magnetic resonance methods can be used to (a) image sessile droplets on structured surfaces and (b) investigate their composition in a time-resolved manner. First it is shown that water droplets on superhydrophobic, hydrophobic and hydrophilic surfaces, despite the large liquid/gas interface, can be imaged well and without interfering artefacts using RARE. Further, the signals are examined in localised PRESS NMR spectra with respect to line shape and quantifiability. Finally, it is demonstrated that non-localised NMR spectra can be used to track the droplet composition during evaporation.

© 2019 Elsevier Inc. All rights reserved.

1. Introduction

Evaporation processes of small droplets on (structured) surfaces (so called sessile droplets) differ significantly from evaporation on a large homogeneous surface. Many different factors have an influence on evaporation processes, with boiling point and vapor pressure of the liquid (mixture) being the most important ones. The evaporation of sessile droplets depends not only on these factors, but also on the macro- and microscopic structure of the surface and its chemical composition, which among other factors affects the contact angle and subsequently the liquid-gas interface of the droplet [1–3]. If the droplet is small enough, the contact angle of the droplet on the surface plays a decisive role in addition to the boiling point and the vapor pressure of the evaporating liquid [1–3]. The contact angle depends, among other things, on the wettability of the surface, which can, for example, be influenced by targeted macroscopic or microscopic structuring or by chemical modification [4,5]. On *stimuli-responsive* surfaces the wettability and/or contact angle can be influenced by a chemical or physical stimulus like mechanical stress [6] or irradiation with UV light [7,8]. Furthermore, contact angles on flat or mesoporous surfaces functionalized with ferrocene polymers can be altered via redox reactions [9,10]. The contact angle on mesoporous surfaces is also determined by the accessibility of the pores [11].

The understanding of evaporation processes of sessile droplets on complex structured surfaces is crucial e.g. to explain the formation of coffee stains [12,13] or to optimize offset printing [14]. In both examples, however, no evaporation of pure substances takes place, since coffee or inks are complex mixtures of substances. As a result, properties such as surface tension, viscosity or hydrophilicity can change during evaporation and thus influence the contact angle. This in turn can affect the evaporation of the droplet [15].

Contact angles of droplets on surfaces are usually investigated using optical methods [16,17]. Such methods are very well suited, for example, to observe macroscopic phase separation in droplets during evaporation [18]. For homogeneous liquid mixtures, the composition of the droplet can be determined indirectly from the contact angle via an appropriate calibration or via measurement of the refractive index [19,20].

* Corresponding author.
E-mail address: jkind@thielelab.de (J. Kind).

https://doi.org/10.1016/j.jmr.2019.106579
1090-7807/© 2019 Elsevier Inc. All rights reserved.

Since a change in contact angle is not necessarily caused by a change in the composition of the droplet, but can also be caused by temperature changes or other factors, such a calibration can only be used to a limited extent. During the evaporation of a liquid, the droplet usually cools down so that temperature gradients can occur in the droplet [21], which can induce convective flows [22,23] and concentration gradients in evaporating droplets [24]. Such processes are often simulated with finite element methods, for example [25–27]. These methods need at least some input parameters like surface tension or the time dependent composition, which might not be known for droplets of complex liquid mixtures.

Thus it would be desirable to investigate the composition of small liquid droplets on surfaces using spectroscopic methods such as NMR spectroscopy and related MR techniques, which have proven that they can be used in medicine, natural sciences and engineering for a variety of applications such as imaging, structure elucidation, rheology, diffusion analysis and many more. The investigation of objects with phase boundaries, especially with a gas/liquid interface, is avoided if possible, since at such interfaces variations in magnetic susceptibility can be present. These usually lead to magnetic field inhomogeneities, which can cause artefacts in MR images and broad signals in NMR spectra. This hampers/prevents quantification and makes imaging of (evaporating) droplets a formidable challenge.

Nevertheless, MR techniques have been used, for example, to study the surface tension of droplets on surfaces in two-phase liquid systems [28]. Also the penetration of water droplets into different asphalts has been investigated by MRI experiments [29] or the freezing of a water droplet by MRI experiments was examined [30]. Recently, Kresse et al. proposed a setup with a static field gradient, for the examination of droplets on surfaces with high resolution in z direction [31]. Besides examination of static systems MR imaging and NMR spectroscopy can be used for the investigation of dynamic processes like e.g. tablet dissolution [32], growth of lithium dendrimers in battery cells [33] or flow in porous systems [34]. However, we are not aware of any studies where pulsed field gradient MR experiments have been used to investigate sessile droplets on functionalized surfaces and their evaporation.

2. Materials and methods

1-Hexanol and acetone were purchased from Sigma Aldrich and used as received.

All MR images and NMR spectra were acquired with a Bruker Avance III HD spectrometer with 400 MHz proton resonance frequency (9.4 T), equipped with a narrow bore micro 5 probe with x, y, z gradients and three GREAT 60 (A) gradient amplifiers. All images and NMR spectra were acquired using an insert with a 10 mm coil tuned to the resonance frequency of ^{1}H. MRI and NMR data were acquired and processed using Paravision 6 and Topspin 3.1, respectively. All experiments were conducted at room temperature. For all experiments standard sequences from the Bruker pulse sequence library were used. Acquisition parameters of MR images and NMR spectra are given in the figure captions.

All samples were prepared in 10 mm NMR tubes (Wilmad Labglas HT WG-4000). Acrylate inserts were 3D printed on a Pico2HD (Asiga) DLP 3D printer using *Plas*CLEAR (Asiga) or Clear Resin BV-007 (MIICRAFT) photo resin. Superhydrophobic silicon nanofilament surfaces were prepared on glass slides according to a literature procedure [35–37]. Hydrophobic PFDTS (Perfuorodecyltrichlorosilane) surfaces were prepared according to a literature procedure on 7 mm round microscopy glasses (Plano) [5,38]. Round microscopy glasses or glass flakes were glued to the 3D printed inserts with cyanoacrylate superglue (Pattex, Henkel).

Photographs were taken with a Canon EOS 1300D with a Canon Zoom Lens EF-s with 18–55 mm focal length (aperture 1:3.5–5.6). The photographs shown were taken with 1/20 s exposure time at iso 1600.

3. Results and discussion

3.1. Sample setup

For the investigation of small droplets on surfaces of different hydrophobicity by NMR and MRI, a method for introducing a horizontal surface and depositing the droplets on this surface in an NMR tube must be developed first. Either a) a flat bottom tube or b) a cylindrical insert with a flat surface for round bottom tubes can be used (Fig. 1). The argument against a) is that the glass bottom lies within the active volume when the droplet is centered in the field of view, which can lead to additional magnetic field inhomogeneities. Therefore, approach b) is pursued. The basic body for such an insert can either be made from commercially available plastic rods with a suitable diameter or from acrylic resins using 3D printing. The advantage of 3D printing compared to commercially available plastic rods is the free choice of diameters, so that an optimal fit of the insert in the NMR tube can be achieved. In order to obtain inserts with different surface properties, a round microscopy glass sheet or silicon wafer with the desired surface properties can be bonded to the base body using superglue.

The deposition of droplets with defined volumes on such surfaces within the NMR tube proves to be difficult. This is mainly due to the fact that droplets are deposited using syringes with long cannulas. Depending on the hydrophobicity of the surface, the droplets roll towards the tube wall when the cannula is moved horizontally, so that the tube wall is wetted. A well-functioning low-tech solution to this problem has been the positioning of the droplet outside the tube and the reduction of the droplet size. In the volume range smaller than 10 μL, droplets can be reproducibly deposited on the surfaces with piston-operated pipettes. Once the droplet has been placed, it can be transferred together with the insert into the NMR tube. Due to the well balanced fit of the 3D printed insert, the insert slowly slides down the tube without the droplet being deformed by sudden changes in velocity.

Drops with volumes between 10 and 2 μL can easily be placed in the tube. With decreasing droplet size, however, the filling factor

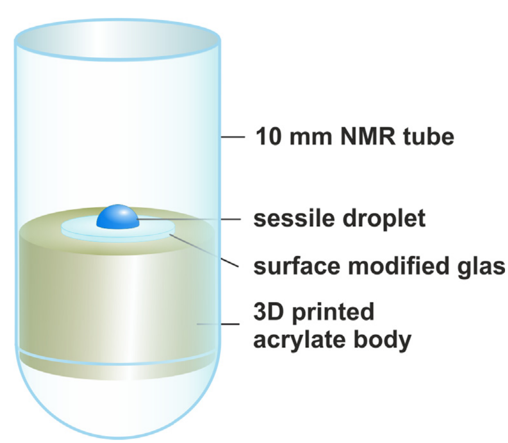

Fig. 1. Sample assembly for the measurement of sessile droplets on planar functionalized surfaces. In the 10 mm NMR tube a 3D printed acrylic cylinder is used, on which functionalized glass plates can be applied and fixed with superglue. The small gap between spacer and tube wall can be filled with liquid, which enhances the filling factor. This might be useful in case when the signal intensity of a small sessile droplet is too low. In all experiments shown in this paper, the tube was left open to the atmosphere.

also decreases. For droplets larger than 4–5 μL, the filling factor is usually large enough to allow all automatic routines (shimming, automatic adjustment of pulse power and receiver gain) to be performed. For droplets smaller than 5 μL, the automatic routines fail more frequently because the absolute signal strength is too low. Such small droplets can still be imaged if the corresponding settings are adjusted manually.

3.2. Droplet shape and artefacts in MR images

Since the shown sample configuration of small droplets on surfaces has both a large curved liquid/gas interface and a flat liquid/solid interface, it is expected that susceptibility artefacts occur in MR images of such samples. Therefore, it was first investigated how MR imaging performs compared (in terms of reproducibility, signal intensity distribution, shape and contact angle) to optical methods like photography in such a challenging sample geometry. In the following, images of small water droplets on a superhydrophobic, a hydrophobic and a hydrophilic surface are shown, which are recorded with FLASH (Fast Low Angle SHot) [39,40] sequences and RARE (RApid imaging with Refocused Echoes) [41] sequences. RARE experiments usually show fewer artefacts in samples with T_2^* inhomogeneities than images obtained by FLASH sequences. This is also observed for the water droplets on hydrophobic and superhydrophobic surfaces (Fig. 2) in the current investigation. Here, the region near the three-phase contact line (substrate/droplet/gas phase) is not reproduced properly in FLASH imaging experiments. This is observed in terms of inhomogeneities in signal intensities, which are much more severe in FLASH than in RARE experiments.

In RARE experiments a more even distribution of the signal intensity over the droplet volume is observed. Most of the curved liquid/gas interface is imaged well with both sequences. In the RARE image of the droplet on the superhydrophobic surface, the liquid/solid interface is slightly curved instead of flat. Both types of sequences yield proper images of the flat water droplet on the hydrophilic surface. The sagittal images of the droplets on the three surfaces obtained from RARE experiments are compared with laterally taken photographs of drops of equal volume on the same three surfaces. For both superhydrophobic and hydrophobic, the RARE image and the photographs show a comparable droplet shape for two droplets of the same volume on the same surface.

Overall, artefact formation is less pronounced than expected, if short TE times are used, MR images can be easily superimposed with photographs. The MR images shown illustrate that MR methods are able to image droplets with a large interface, so that e.g. contact angles can be determined. Nevertheless, optical methods are still superior to MR methods in terms of image resolution and measurement time. MR methods, however, offer the possibility to investigate the chemical composition of a droplet directly. Although the magnetic field is homogeneous enough for clean RARE images, in the following section the magnetic field homogeneity in the droplets will be further investigated, since for determining compound ratios using non-localised and localised spectroscopy more homogeneous fields are needed than for imaging only.

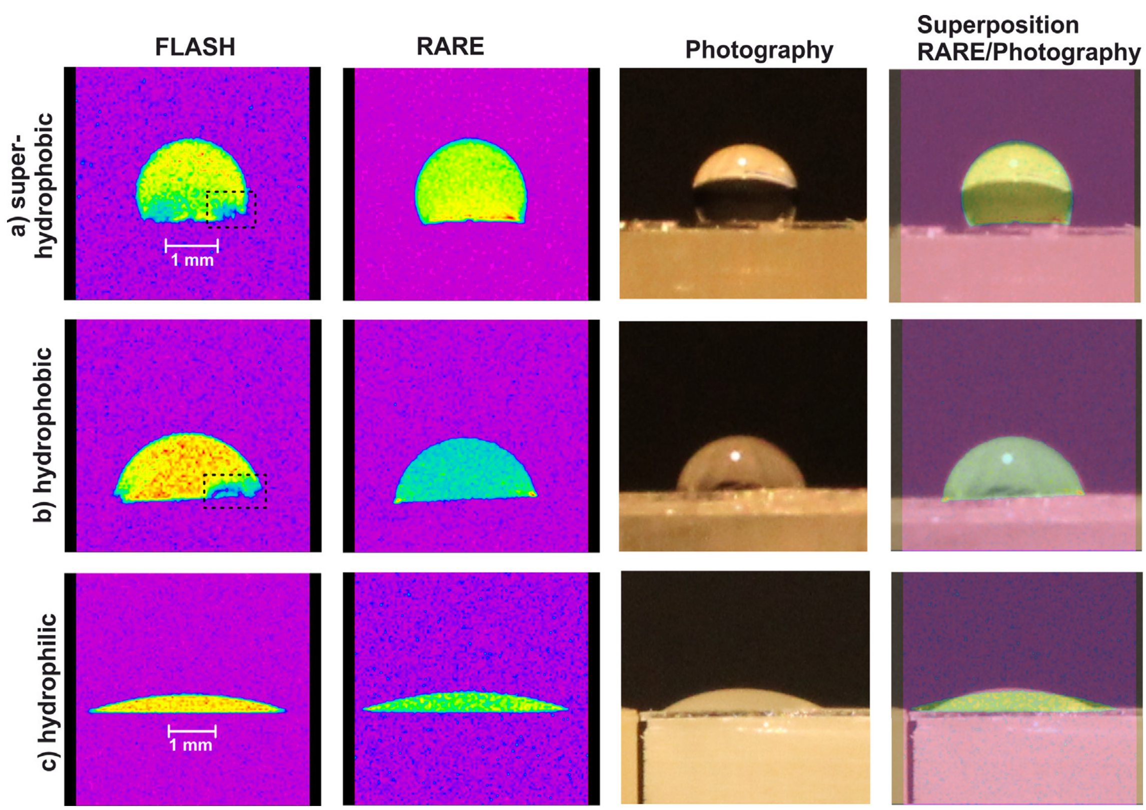

Fig. 2. FLASH and RARE images as well as photographs of water droplets on a (a) superhydrophobic (silicon nano filament), (b) hydrophobic (PFDTS) and (c) hydrophilic (silicate glass) surfaces. Signal distribution inhomogenieties in the FLASH images of the water droplets on the superhydrophobic and hydrophobic surfaces are marked with dashed boxes. FLASH and RARE images (a) and (b) were acquired with 4.5 mm FOV (Field of View) with a matrix of 100 × 100 voxel and a slice thickness of 0.75 mm. RARE images were acquired with NS = 4, TR = 2000 ms, echo time = 20 ms and a RARE factor of 8 within a total acquisition time of 1 min 36 s per image. FLASH images were acquired with NS = 3, 30° excitation angle, echo time = 4 ms and TR = 300 ms within a total acquisition time of 1 min 30 s per image. FLASH and RARE images of (c) were acquired with a FOV of 5 mm, a matrix of 110 × 110 voxel and a slice thickness of 0.75 mm. The RARE image was acquired with NS = 4, TR = 2000 ms and echo time = 20 ms within 1 min 44 s per image and the FLASH image with NS = 4, 30° excitation angle and TR = 300 ms within 2 min 12 s per image.

3.3. Magnetic field inhomogenieties in small droplets

Magnetic field homogeneity within droplets can be examined by recording T_2* and T_2 weighted images and comparing these images. It is assumed that the magnetic field within a water droplet with a large liquid/gas interface is less homogeneous than in a bulk water sample without interfaces. For a droplet of a pure substance, it can be assumed that the droplet has a homogeneous T_2 field, since the mobility of the molecules in the droplet is comparable at any position if temperature gradients are neglected. This can be observed for a water droplet on the PFDTS surface, where a MSME (Multi Slice Multi Echo) [42,43] image shows homogeneous signal decay with a T_2 of 74.1 ms (Fig. 3c, ROI 2) with slightly higher T_2 times of 94.7 ms near the three phase contact line (Fig. 3c, ROI 1). Therefore, inhomogeneous signal intensities in T_2*-weighted images are mainly due to magnetic field inhomogeneities. T_2* can be measured by recording GRE (Gradient Echo) experiments [44]. For the water droplet on the hydrophobic PFDTS surface (Fig. 3a) in such multi gradient echo (MGE) experiments inhomogeneous signal decays with T_2* between 6.2 ms (ROI 1) and 12.5 ms (ROI 2) are observed, which indicate corresponding magnetic field inhomogeneities, especially near the three phase contact line. Fieldmap shim routines can be used to reduce the occurring field inhomogeneity (Fig. 3b) to a certain extent. This routine improves the field homogeneity in the center of the droplet significantly (T_2* = 24.5 ms in ROI 1 and 24.1 in ROI 2), whereas strong field inhomogeneities remain near the three phase contact line. Fits of T_2* and T_2 are given in the supporting information.

The comparison of MSME and MGE echo images and calculated T_2* and T_2 times shows, that a severe variation in the magnetic field strength is present within the droplet, even after field map shimming of the sample. As shown in Section 3.2 (Fig. 2) and this section in Fig. 3c, this is not a severe problem for imaging of sessile droplets as spin echo experiments like MSME or RARE experiments with short TE times can be used. Both experiments yield images with evenly distributed signal intensity and the liquid/gas and liquid/solid interfaces are imaged properly. However, the presence of an inhomogeneous T_2* distribution within the droplet can have negative effects on localised NMR spectroscopy, as line shape are directly correlated with T_2*. Therefore, line shapes of non-localised and localised NMR spectra of sessile droplets were examined.

3.4. Line shapes in non-localised and localised NMR spectroscopy

As shown in Section 3.2, RARE experiments (and other spin echo experiments with short TE times) can be used to image droplets placed on planar surfaces without disturbing T_2* artefacts. To investigate the composition of droplets, however, not only images with defined interfaces are required, but also NMR spectra from which the composition can be determined by chemical shift resolution are necessary. In order to obtain spectra with narrow lines, usually a higher magnetic field homogeneity and longer T_2 times are required than for the generation of good MR images, as the experimental linewidth over the full width at half-height (FWHH) (for a single exponential decay) depends on T_2* (Eq. (1)). T_2* depends on T_2 and the additional dephasing due to field inhomogenieties ($T_{\text{inhomo.}}$) as shown in Eq. (2) [45]. The reciprocal T_2^{-1} is proportional to the deviation ΔB_0 of the magnetic field and the gyromagnetic ratio of the nucleus observed.

$$FWHH = \frac{1}{\pi \cdot T_2^*} \tag{1}$$

$$\frac{1}{T_2^*} = \frac{1}{T_2} + \frac{1}{T_{inhomo.}} = \frac{1}{T_2} + \gamma \cdot \Delta B_0 \tag{2}$$

Therefore, in the following section simple single pulse (NSPECT, Non-localised SPECTroscopy) and spatially resolved (PRESS, Point RESolved Spectroscopy) [46,47] NMR spectra of sessile droplets

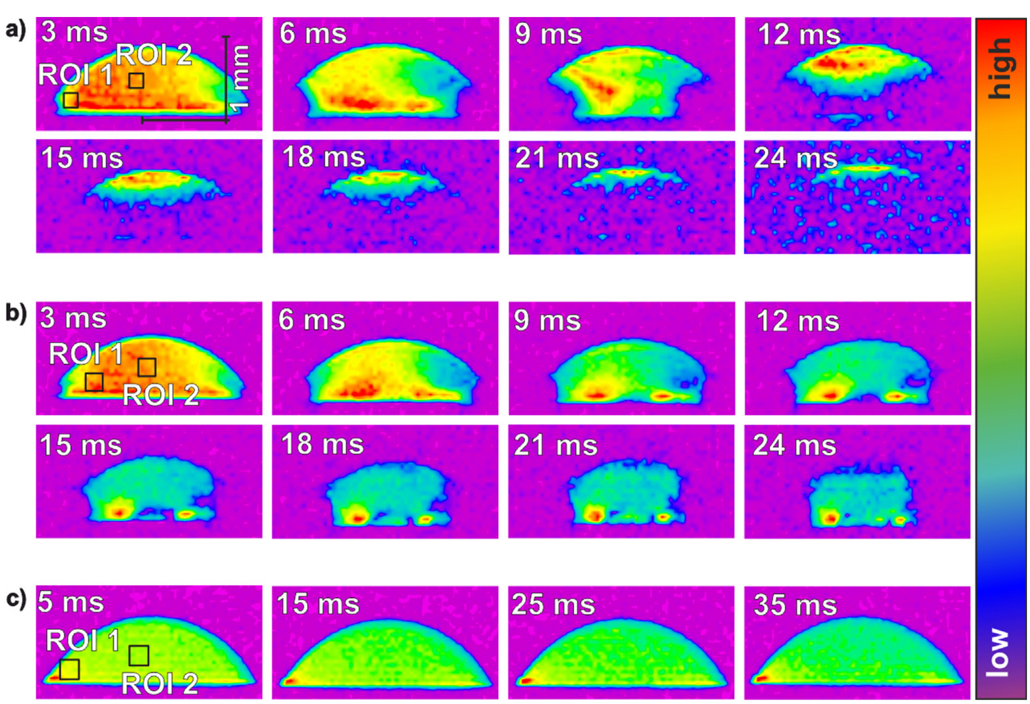

Fig. 3. (a) MGE images at different echo times of a 4.5 μL water droplet on the hydrophobic PFDTS surface, acquired with TR = 2000 ms, NS = 4, FOV = 4.5 × 4.5 mm (80 × 80 matrix), 0.75 mm slice thickness and TE = 3 ms. (b) MGE images of the same droplet after field map shim procedure. (c) MSME echo images at different echo times of the same droplet acquired with an echo spacing of 5 ms, TR = 2000 ms, NS = 4, FOV = 4.5 × 4.5 mm (90 × 90 matrix), 0.75 mm slice thickness. All images are cropped to approx. 1.25 × 2.75 mm.

are examined in terms of line shape and quantifiability of the signal integrals. The focus will be on the impact of different voxel sizes/-geometries, as well as on using signals with chemical shift differences for quantification of signal integrals.

As shown in Section 3.2 the droplet shape in MR images was examined using water droplets. For the analysis of line shapes non-localised (NSPECT) and locally (PRESS) recorded NMR spectra, both water and 1-hexanol droplets were investigated. Hexanol was chosen because of its more complex spectrum compared to water, so that a) the chemical shift resolution at the given field homogeneity and b) the quantifiability of the relative integrals in NSPECT and PRESS spectra of one component can be examined. This is important to ensure the accuracy of a composition analysis over the relative integral of two or more species in complex mixtures. Small droplets (ca. 5 μL) of both liquids water and 1-hexanol do evaporate on a timescale of up to several days at RT in open NMR tubes, so that no significant change in the droplet volume is expected for the experiments in the following sections.

3.4.1. Impact of voxel size

PRESS experiments were performed on small water droplets with different voxel sizes. It is expected, that the line width can be reduced by choosing smaller voxels, as the extent of magnetic field inhomogenieties should be smaller in small voxels compared to bigger voxels, so that the average T_2* should be larger [48,49]. Prior to acquisition of PRESS spectra, a RARE image of the droplet is acquired and automatic shim procedure as well as field map shimming is applied to the sample. For validation of the assumption that for smaller voxels smaller line widths are obtained, no voxel specific shimming is applied prior to measurement of PRESS spectra.

These line shape tests were performed within the center of a 4.2 μL water droplet on a PFDTS surface and near the three phase contact line of this droplet. Measurements of PRESS spectra in the center show that the reduction of voxel sizes does improve the line width of the water resonance from 18.3 Hz FWHH (37.6 Hz FWTH) for a 0.7 mm × 0.7 mm × 0.7 mm voxel to 8 Hz FWHH (20.1 Hz FWTH = Full Width Tenth Height) for a 0.4 mm × 0.4 mm × 0.4 mm voxel and 4.9 Hz FWHH (9.6 Hz FWTH) for a 0.4 mm × 0.4 mm × 0.4 mm voxel (Fig. 4).

Near the three phase contact line the line width of the water resonance is significantly larger than in the center of the droplet. The PRESS spectrum of a 0.4 mm × 0.4 mm × 0.4 mm voxel shows a line width of 167 Hz FWHH. A reduction to a voxel volume of 0.2 mm × 0.2 mm × 0.2 mm voxel reduces the line width to 111 Hz (see SI). Further reducing the voxel size may reduce the line width at the expanse of a significantly longer measurement time.

As expected the line width of PRESS spectra can be reduced by reduction of the voxel size. Hence, it is recommended to use small voxel size for the acquisition of NMR spectra near the three phase contact line.

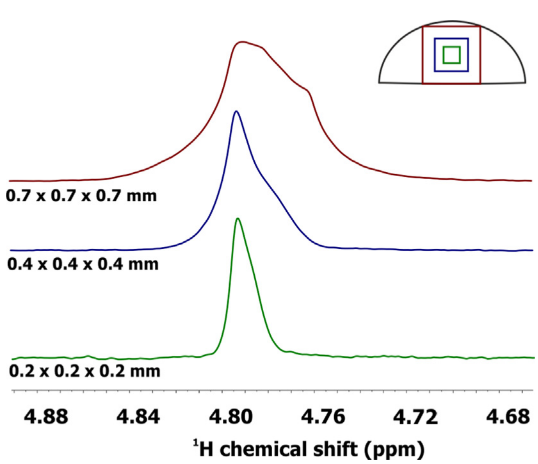

Fig. 4. PRESS ^{1}H NMR spectra of a 4.2 μL water droplet on a hydrophobic PFDTS surface measured within isotropic voxels. Position of the voxel is indicated in the drawing in the right upper corner. All spectra were acquired with 8096 data points within 1.01 s acquisition time. A relaxation delay of 2 s was used for all measurements. For the spectrum with the 0.7 × 0.7 × 0.7 mm voxel (0.343 mm^3, red) two scans were accumulated within a total experimental time of 4 s, for the spectrum with the 0.4 × 0.4 × 0.4 mm voxel (0.064 mm^3, blue) 8 scans were accumulated within a total experimental time of 16 s and for the spectrum with the 0.2 × 0.2 × 0.2 mm voxel (0.008 mm^3, green) 32 scans were accumulated within a total experimental time of 1 min 4 s. (For interpretation of the references to colour in this figure legend, the reader is referred to the web version of this article.)

3.4.2. Chemical shift resolution and Quantifiability:

1-Hexanol was chosen as the chemical shift resolution can be well investigated by separation of the CH_2 and CH_3 resonances. NSPECT and PRESS spectra of a small 1-hexanol droplet were recorded on the hydrophobic PFDTS surface (Fig. 5; for RARE image of the droplet see SI). In both spectra resonances with line widths greater than 50 Hz were observed. The PRESS spectrum recorded in a 0.4 × 0.4 × 2 mm voxel shows slightly narrower lines and a more uniform line shape. In both spectra resonances of the —O—CH_2— and CH_2/CH_3 groups are baseline separated and can therefore be integrated separately. The quantifiability of both spectra can be judged by the deviation of the measured integral from the ideal distribution of 2:11 expected for 1-hexanol.

In the non-localised NSPECT ^{1}H NMR spectrum a relation between the integral of the —O—CH_2— and the —CH_2—/—CH_3 resonances of 1.86:11 instead the ideal relation of 2:11 is observed. Also the signal integral of the OH resonance with a value of 0.96 deviates by 4% from the ideal value. Both deviations can be explained by the processing needed to obtain a spectrum with a clean baseline, as a Whittaker smoother [50] has to be applied to correct the baseline of the NSPECT spectrum (for uncorrected spectrum see SI, Fig. S4). The PRESS spectrum acquired in a 0.4 × 0.4 × 2 mm voxel shows a slightly improved and more symmetrical line shape compared to the NSPECT spectrum acquired over the whole droplet. However, the relative integrals are the —O—CH_2— and the —CH_2—/—CH_3 resonances show a ratio of 1.68:11 instead the ideal relation of 2:11 is observed. This increas-

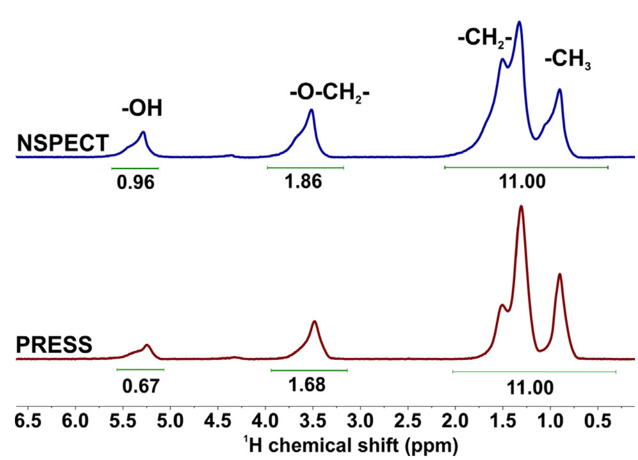

Fig. 5. NSPECT ^{1}H NMR spectrum (blue) of a 4.2 μL 1-hexanol droplet on a PFDTS surface, acquired with 16 k data points (acquisition time = 2 s) and NS = 1. The full width at half height of the —O—CH_2-resonance is ~95 Hz. PRESS ^{1}H NMR spectrum (red) of the same droplet acquired with 16 k data points (acquisition time = 2 s) within a 0.4 × 0.4 × 2 mm voxel and NS = 128 (TR = 10 s). FWHH of the —O—CH_2-resonance is ~75 Hz. (For interpretation of the references to colour in this figure legend, the reader is referred to the web version of this article.)

ing deviation of the relative integrals might be explained by additional signal attenuation caused by T_1/T_2 relaxation occurring during the PRESS sequence [46].

Although both NSPECT and PRESS spectra show wide lines (compared to HR NMR spectroscopy) are observed when measuring sessile droplets, both methods are suitable for qualitative evaluation of the composition of sessile droplets. A NSPECT spectrum is better suited for quantifying the global composition of such droplets with a higher accuracy of approx. 95%. Using non-localised spectroscopy also avoids increasing measurement time.

3.5. Measuring droplet dynamics – Evaporation of droplets formed by binary mixtures

As mentioned in the previous section, the evaporation rate of a small droplet determines the temporal resolution with which evaporation processes can be examined using MR techniques. The evaporation process of small droplets (around 5 μL) consisting of water or alcohols such as 1-hexanol occurs in open NMR tubes on the time scale of days. The evaporation rate could be increased by a gas stream passing over the droplet. In order to investigate faster processes without modifying the setup, droplets from liquids with lower boiling points were examined. As a benchmark for faster processes, a droplet of a binary mixture of water/acetone on a PFDTS surface with acetone being the more volatile component was studied. A rapid decrease of the droplet size caused by the evaporation of acetone can be observed on the time scale of hours (Fig. 6). The evaporation of the droplet occurs with a constant contact angle. In the series of images shown, it can be seen that the change in droplet size has no negative effect on the image quality. Thus, it is assumed that the magnetic field homogeneity does not change significantly during evaporation.

The evolution of the acetone fraction in the droplet can be observed by non-localised NMR spectroscopy (Fig. 7). The line shape in the non-localised recorded spectra varies slightly during the evaporation process, but no strong widening or tailing of the signals is observed. The ratio of water and acetone resonances can be used to calculate the fraction of acetone in the droplet (Fig. 8). If this fraction is plotted against time, an exponential decrease of the acetone fraction is observed. After several hours the remaining droplet consists of pure water.

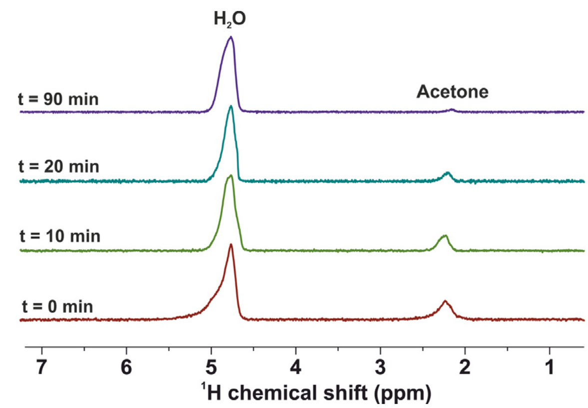

Fig. 7. (global) ^{1}H NMR spectra acquired during evaporation of a water/acetone sessile droplet on a PFDTS surface. Proton chemical shifts were referenced to the acetone resonance.

The data obtained from NMR spectra and MR images can be correlated. For example, the time-dependent droplet height and width or the droplet volume can be compared with the decay of the acetone fraction within the droplet after normalisation of the fraction or width respectively (Fig. 8).

Both the normalised fraction and the droplet width can be fitted with an exponential decay as a very simple model for the decrease of acetone and droplet width during evaporation, neglecting the slow evaporation of water.

$$I(t) = I(0) \cdot e^{-k \cdot t}$$

As a result a rate constants k of 2.45 h^{-1} for the molar fraction and 1.87 h^{-1} for the droplet width are obtained. The correlation between molar ratio of acetone and droplet width is to be expected, as the volume decrease is due to the evaporation of acetone from the droplet, evaporation of water within this time interval can be neglected. After the complete evaporation of acetone the shrinkage rate of the remaining water droplet significantly decreases. This shows that MR imaging and non-localised NMR spectroscopy can be used to observe the shape (via imaging) and the composition (via spectroscopy) of sessile droplets during dynamic processes.

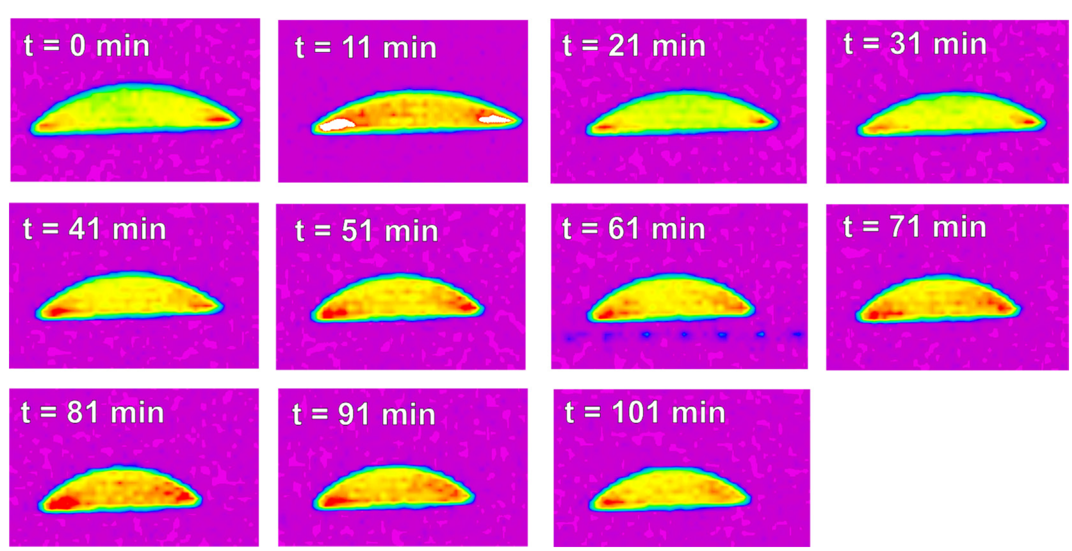

Fig. 6. Series of RARE images during the evaporation of acetone from a 5 μL droplet of a water/acetone mixture on a PFDTS surface. The image acquired at t = 61 min shows an artefact caused by picking up a continuous wave signal emitted by a 400 MHz spectrometer in the neighborhood. Fortunately this artefact does not overlap with the signals of the observed droplet.

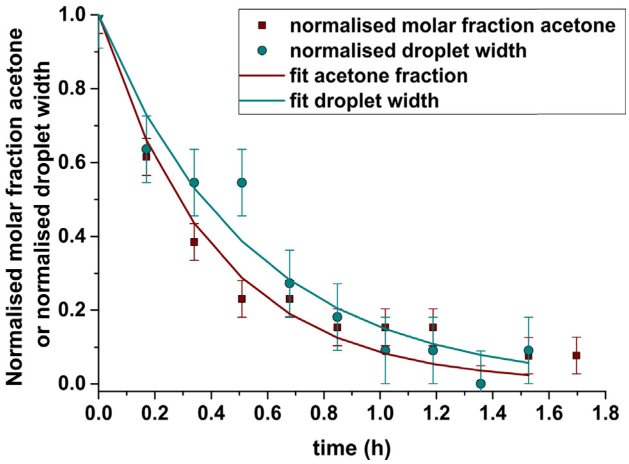

Fig. 8. Normalised molar fraction of acetone and normalised droplet width during the evaporation of a droplet composed of water and acetone. Errors are estimated to be 5% for the molar fraction of acetone and 9% (accuracy was estimated to be +/− three voxels) for the droplet width.

4. Conclusion

In this work it was shown for the first time that MR techniques can be used to image small droplets with volumes between 2 and 10 μL on superhydrophobic, hydrophobic and hydrophilic surfaces. The samples are prepared on 3D printed spacers with a functionalized surface and are transferred into the NMR tube. For future work, this setup can be modified so that (a) the surface is heated or (b) a gas stream passes over the droplet so that the time scales of evaporation processes can be actively controlled. Water droplets can be imaged with well-defined phase boundaries by using spin echo sequences like RARE or MSME with short TE times. These images are perfectly superimposable with laterally acquired photographs and thus demonstrate reproducible droplet deposition as well as the excellent imaging capabilities with very little imhomogenieties. Gradient echo sequences like FLASH also yield images with well-defined liquid-gas interfaces, but homogeneity of signal intensities near the three phase contact line is much more inhomogeneous than in spin echo experiments like RARE images, due to inhomogeneous and short T_2^* times. Magnetic field homogeneity within a water droplet on a hydrophobic PFDTS surface was examined with sagittally acquired MGE experiment, which showed a fast and inhomogeneous signal decay over the droplet. Field map shimming improves the signal homogeneity in the center of the droplet, but near the three phase contact line, a significant inhomogeneity in the signal decay remains.

The major advantage of MR techniques compared to optical methods is the possibility to spectroscopically study the composition of droplets. Here it was shown that with the magnetic field homogeneities present in the droplet sufficiently good NMR spectra of water or 1-hexanol can be obtained. However, short T_2^* times lead to broad lines (>100 Hz) in ^{1}H spectra near the three phase contact line. A reduction of the voxel size improves the line width obtained, so that a higher chemical shift resolution can be obtained at the expanse of a longer acquisition time. It is recommended that voxel specific shimming is applied. Nevertheless, the spectral quality is good enough, that non-localised and spatially resolved NMR spectroscopy can be applied to qualitative and quantitative examination of droplets consisting of complex liquids of static samples.

This allows e.g. the investigation of evaporation processes of small droplets from liquid mixtures, e.g. water/acetone as model system. Here we show that the composition of a 5 μL droplet composed of water and acetone can be tracked during the evaporation of acetone on the timescale of hours by using non-localised spectroscopy. In parallel RARE images can be acquired so that the droplet width or heights can be tracked and compared with the changes of the droplet composition. This is of great interest, since the understanding of the evaporation of small droplets is essential for e.g. the optimization of offset printing.

5. Notes

Raw data are available under http://doi.org/10.23728/b2share.5f4f0b7ae6d84ab8bdab95131d6ed0a3.

Acknowledgements

The authors thank Florian Geyer (MPIP Mainz) for preparation of the superhydrophobic silicon nanofilament surfaces and Maximilian Hartmann (Institute for Nano- and Microfluidics (NMF), TU Darmstadt) for the preparation of the hydrophobic PFDTS surfaces. Additionally, we thank Alena Bell (Stark Group, TU Darmstadt) for 3D printing of the spacers. The authors thank Melanie Britton for a fruitful discussion.

We kindly acknowledge the financial support by the German Research Foundation (DFG) within the Collaborative Research Centre 1194 "Interaction of Transport and Wetting Processes", Project A08.

Appendix A. Supplementary material

Supplementary data to this article can be found online at https://doi.org/10.1016/j.jmr.2019.106579.

References

[1] C. Bourges-Monnier, M.E.R. Shanahan, Influence of evaporation on contact angle, Langmuir 11 (7) (1995) 2820–2829.
[2] S. Chandra, M. di Marzo, Y.M. Qiao, P. Tartarini, Effect of liquid-solid contact angle on droplet evaporation, Fire Saf. J. 27 (2) (1996) 141–158.
[3] J.K. Park, J. Ryu, B.C. Koo, S. Lee, K.H. Kang, How the change of contact angle occurs for an evaporating droplet: effect of impurity and attached water films, Soft Matter 8 (47) (2012) 11889–11896.
[4] J. Wang, M. Do-Quang, J.J. Cannon, F. Yue, Y. Suzuki, G. Amberg, J. Shiomi, Surface structure determines dynamic wetting, Sci. Rep. 5 (2015) 8474.
[5] M. Hartmann, S. Hardt, Stability of evaporating droplets on chemically patterned surfaces, Langmuir 35 (14) (2019) 4868–4875.
[6] X. Huang, Y. Sun, S. Soh, Stimuli-responsive surfaces for tunable and reversible control of wettability, Adv. Mater. (Weinheim, Ger.) 27 (27) (2015) 4062–4068.
[7] S. Samanta, J. Locklin, Formation of photochromic spiropyran polymer brushes via surface-initiated, ring-opening metathesis polymerization: reversible photocontrol of wetting behavior and solvent dependent morphology changes, Langmuir 24 (17) (2008) 9558–9565.
[8] W. Jiang, G. Wang, Y. He, X. Wang, Y. An, Y. Song, L. Jiang, Photo-switched wettability on an electrostatic self-assembly azobenzene monolayer, Chem. Commun. 28 (2005) 3550–3552.
[9] J. Elbert, M. Gallei, C. Rüttiger, A. Brunsen, H. Didzoleit, B. Stühn, M. Rehahn, Ferrocene polymers for switchable surface wettability, Organometallics 32 (20) (2013) 5873–5878.
[10] J. Elbert, F. Krohm, C. Rüttiger, S. Kienle, H. Didzoleit, B.N. Balzer, T. Hugel, B. Stühn, M. Gallei, A. Brunsen, Polymer-modified mesoporous silica thin films for redox-mediated selective membrane gating, Adv. Funct. Mater. 24 (11) (2014) 1591–1601.
[11] L. Silies, E. Gonzalez Solveyra, I. Szleifer, A. Andrieu-Brunsen, Insights into the role of counterions on polyelectrolyte-modified nanopore accessibility, Langmuir 34 (20) (2018) 5943–5953.
[12] M. Majumder, C.S. Rendall, J.A. Eukel, J.Y.L. Wang, N. Behabtu, C.L. Pint, T.-Y. Liu, A.W. Orbaek, F. Mirri, J. Nam, A.R. Barron, R.H. Hauge, H.K. Schmidt, M. Pasquali, Overcoming the "Coffee-Stain" effect by compositional marangoni-flow-assisted drop-drying, J. Phys. Chem. B 116 (22) (2012) 6536–6542.
[13] T. Breinlinger, T. Kraft, A simple method for simulating the coffee stain effect, Powder Technol. 256 (2014) 279–284.
[14] T. Lim, J. Jeong, J. Chung, J.T. Chung, Evaporation of inkjet printed pico-liter droplet on heated substrates with different thermal conductivity, J. Mech. Sci. Technol. 23 (7) (2009) 1788–1794.
[15] N.M. Kovalchuk, A. Trybala, V.M. Starov, Evaporation of sessile droplets, Curr. Opin. Colloid Inter. Sci. 19 (4) (2014) 336–342.

[16] A.W. Neumann, R.J. Good, Techniques of Measuring Contact Angles, in: R.J. Good, R.R. Stromberg (Eds.), Surface and Colloid Science: Volume 11: Experimental Methods, Springer US, Boston, MA, 1979, pp. 31–91.
[17] M. Schmitt, F. Heib, High-precision drop shape analysis on inclining flat surfaces: Introduction and comparison of this special method with commercial contact angle analysis, J. Chem. Phys. 139 (13) (2013) 134201.
[18] H. Tan, C. Diddens, P. Lv, J.G.M. Kuerten, X. Zhang, D. Lohse, Evaporation-triggered microdroplet nucleation and the four life phases of an evaporating Ouzo drop, Proc. Natl. Acad. Sci. U.S.A. 113 (31) (2016) 8642–8647.
[19] Jarray, A.; Magnanimo, V.; Luding, S., Wet granular flow control through liquid induced cohesion, 2018.
[20] J. Wilms, B. Weigand, Composition measurements of binary mixture droplets by rainbow refractometry, Appl. Opt. 46 (11) (2007) 2109–2118.
[21] R.J. Hopkins, C.R. Howle, J.P. Reid, Measuring temperature gradients in evaporating multicomponent alcohol/water droplets, Phys. Chem. Chem. Phys. 8 (24) (2006) 2879–2888.
[22] M.R. Barmi, C.D. Meinhart, Convective flows in evaporating sessile droplets, J. Phys. Chem. B 118 (9) (2014) 2414–2421.
[23] S. Karpitschka, F. Liebig, H. Riegler, Marangoni contraction of evaporating sessile droplets of binary mixtures, Langmuir: ACS J. Surf. Coll. 33 (19) (2017) 4682–4687.
[24] A.-M. Cazabat, G. Guéna, Evaporation of macroscopic sessile droplets, Soft Matter 6 (12) (2010) 2591–2612.
[25] C. Diddens, Detailed finite element method modeling of evaporating multi-component droplets, J. Comput. Phys. 340 (2017) 670–687.
[26] C. Diddens, J.G.M. Kuerten, C.W.M. van der Geld, H.M.A. Wijshoff, Modeling the evaporation of sessile multi-component droplets, J. Coll. Inter. Sci. 487 (2017) 426–436.
[27] A. Maatar, S. Chikh, M. Ait Saada, L. Tadrist, Transient effects on sessile droplet evaporation of volatile liquids, Int. J. Heat Mass Trans. 86 (2015) 212–220.
[28] R. Hussain, S.J. Vogt, A. Honari, K.G. Hollingsworth, A.J. Sederman, J. Mitchell, M.L. Johns, Interfacial tension measurements using MRI drop shape analysis, Langmuir 30 (6) (2014) 1566–1572.
[29] F.P. Miknis, A.T. Pauli, A. Beemer, B. Wilde, Use of NMR imaging to measure interfacial properties of asphalts, Fuel 84 (9) (2005) 1041–1051.
[30] J.P. Hindmarsh, C. Buckley, A.B. Russell, X.D. Chen, L.F. Gladden, D.I. Wilson, M. L. Johns, Imaging droplet freezing using MRI, Chem. Eng. Sci. 59 (10) (2004) 2113–2122.
[31] B. Kresse, M.V. Höfler, A.F. Privalov, M. Vogel, One dimensional magnetic resonance microscopy with micrometer resolution in static field gradients, J. Magn. Reson. 106566 (2019).
[32] K.P. Nott, Magnetic resonance imaging of tablet dissolution, Eur. J. Pharm. Biopharm. 74 (1) (2010) 78–83.
[33] A.J. Ilott, M. Mohammadi, H.J. Chang, C.P. Grey, A. Jerschow, Real-time 3D imaging of microstructure growth in battery cells using indirect MRI, Proc. Natl. Acad. Sci. U.S.A. 113 (39) (2016) 10779.
[34] M.M. Britton, Applications of magnetic resonance imaging to probe chemistry and flow in complex systems, in: Nuclear Magnetic Resonance: Volume 45, The Royal Society of Chemistry, 2016, pp. 164–189.
[35] G.A. Lorigan, R.E. Minto, W. Zhang, Teaching the fundamentals of pulsed NMR spectroscopy in an undergraduate physical chemistry laboratory, J. Chem. Educ. 78 (7) (2001) 956.
[36] F. Geyer, C. Schönecker, H.-J. Butt, D. Vollmer, CO2 capture: enhancing CO2 capture using robust superomniphobic membranes (adv. mater. 5/2017), Adv. Mater. (Weinheim, Ger.) 29 (5) (2017).
[37] F. Geyer, M. D'Acunzi, C.-Y. Yang, M. Müller, P. Baumli, A. Kaltbeitzel, V. Mailänder, N. Encinas, D. Vollmer, H.-J. Butt, How to coat the inside of narrow and long tubes with a super-liquid-repellent layer—a promising candidate for antibacterial catheters, Adv. Mater. (Weinheim, Ger.) 31 (2) (2019) 1801324.
[38] T.M. Mayer, M.P.D. Boer, N.D. Shinn, P.J. Clews, T.A. Michalske, Chemical vapor deposition of fluoroalkylsilane monolayer films for adhesion control in microelectromechanical systems, J. Vac. Sci. Technol., B: Microelectron. Nanometer Struct.–Process., Meas., Phenom. 18 (5) (2000) 2433–2440.
[39] J. Frahm, A. Haase, D. Matthaei, Rapid NMR imaging of dynamic processes using the FLASII technique, Magn. Reson. Med. 3 (2) (1986) 321–327.
[40] A. Haase, J. Frahm, D. Matthaei, W. Hanicke, K.D. Merboldt, FLASH imaging. Rapid NMR imaging using low flip-angle pulses, J. Mag. Reson. 67 (2) (1986) 258–266.
[41] J. Hennig, A. Nauerth, H. Friedburg, RARE imaging: a fast imaging method for clinical MR, Magn. Reson. Med. 3 (6) (1986) 823–833.
[42] S. Majumdar, S.C. Orphanoudakis, A. Gmitro, M. O'Donnell, J.C. Gore, Errors in the measurements of T2 using multiple-echo MRI techniques. II. Effects of static field inhomogeneity, Magn. Reson. Med. 3 (4) (1986) 562–574.
[43] A.P. Crawley, R.M. Henkelman, Errors in T2 estimation using multislice multiple-echo imaging, Magn. Reson. Med. 4 (1) (1987) 34–47.
[44] G.B. Chavhan, P.S. Babyn, B. Thomas, M.M. Shroff, E.M. Haacke, Principles, techniques, and applications of T2*-based MR imaging and its special applications, Radiographics 29 (5) (2009) 1433–1449.
[45] T.D.W. Claridge, Introducing high-resolution NMR, in: T.D.W. Claridge (Ed.), Tetrahedron Organic Chemistry Series, Elsevier, 2009, pp. 11–34 (Chapter 2).
[46] C.T.W. Moonen, M.V. Kienlin, P.C.M. Van Zijl, J. Cohen, J. Gillen, P. Daly, G. Wolf, Comparison of single-shot localization methods (steam and press) for In vivo proton NMR spectroscopy, NMR Biomed. 2 (5–6) (1989) 201–208.
[47] U. Klose, Measurement sequences for single voxel proton MR spectroscopy, Eur. J. Radiol. 67 (2) (2008) 194–201.
[48] A. Bax, R. Freeman, Enhanced NMR resolution by restricting the effective sample volume, J. Mag. Reson. 37 (1) (1980) 177–181.
[49] J. Kind, C.M. Thiele, Still shimming or already measuring? – Quantitative reaction monitoring for small molecules on the sub minute timescale by NMR, J. Magn. Reson. 260 (2015) 109–115.
[50] C. Cobas, Applications of the Whittaker smoother in NMR spectroscopy, Magn. Reson. Chem. 56 (12) (2018) 1140–1148.